NEOPLASIA
www.neoplasia.com
Volume 23 Number xxx Month 2021 pp. 624–633

Original Research

The synergy of BET inhibitors with aurora A kinase inhibitors in *MYCN*-amplified neuroblastoma is heightened with functional TP53☆,☆☆

Joanna S. Yi[a,b,*]; Oscar Sias-Garcia[a]; Nicole Nasholm[c]; Xiaoyu Hu[a]; Amanda Balboni Iniguez[b,e,f]; Matthew D. Hall[g]; Mindy Davis[g]; Rajarshi Guha[g]; Myrthala Moreno-Smith[a]; Eveline Barbieri[a]; Kevin Duong[a]; Jessica Koach[c,d,i]; Jun Qi[e,f,h]; James E. Bradner[e,f,h]; Kimberly Stegmaier[b,e,f]; William A. Weiss[c,d,i]; W. Clay Gustafson[c,d,*]

[a] Department of Pediatrics, Section of Hematology-Oncology, Texas Children's Cancer and Hematology Centers, Baylor College of Medicine, Houston, Texas, USA
[b] Department of Pediatric Oncology, Dana-Farber Cancer Institute and Boston Children's Hospital, Boston, Massachusetts, USA
[c] Department of Pediatrics, Helen Diller Family Comprehensive Cancer Center, University of California, San Francisco, California, USA
[d] Helen Diller Family Comprehensive Cancer Center, University of California, San Francisco, California, USA
[e] Broad Institute, Cambridge, Massachusetts, USA
[f] Harvard Medical School, Boston, Massachusetts, USA
[g] National Center for Advancing Translational Sciences, National Institutes of Health, Rockville, Maryland, USA
[h] Department of Medical Oncology, Dana-Farber Cancer Institute, Boston, Massachusetts, USA
[i] Department of Neurology and Neurological Surgery, University of California, San Francisco, California, USA

Abstract

Amplification of *MYCN* is a poor prognostic feature in neuroblastoma (NBL) indicating aggressive disease. We and others have shown BET bromodomain inhibitors (BETi) target *MYCN* indirectly by downregulating its transcription. Here we sought to identify agents that synergize with BETi and to identify biomarkers of resistance. We previously performed a viability screen of ~1,900 oncology-focused compounds combined with BET bromodomain inhibitors against *MYCN*-amplified NBL cell lines. Reanalysis of our screening results prominently identified inhibitors of aurora kinase A (AURKAi) to be highly synergistic with BETi. We confirmed the anti-proliferative effects of several BETi+AURKAi combinations in *MYCN*-amplified NBL cell lines. Compared to single agents, these combinations cooperated to decrease levels of N-myc. We treated both *TP53*-wild type and mutant, *MYCN*-amplified cell lines with the BETi JQ1 and the AURKAi Alisertib. The combination had improved efficacy in the *TP53*-WT context, notably driving apoptosis in both genetic backgrounds. JQ1+Alisertib combination treatment of a *MYCN*-amplified, *TP53*-null or *TP53*-restored genetically engineered mouse model of NBL prolonged survival better than either single agent. This was most profound with

Abbreviations: NBL, neuroblastoma; BETi, BET bromodomain inhibitor(s); AURK, aurora kinase; AURKAi, aurora A kinase inhibitor(s); MIPE, Mechanism Interrogation PlatE.

* Corresponding author.
E-mail addresses: Joanna.yi@bcm.edu (J.S. Yi), Clay.Gustafson@ucsf.edu (W.C. Gustafson).

☆ Funding: This work was supported by Hyundai Hope on Wheels Scholar Award, Alex's Lemonade Stand Centers of Excellence Developmental Therapeutics Scholar Award, and NIH Texas Children's Cancer and Hematology Centers K12 Clinical Pharmacology Scholar Award (JSY). NIH R01NS088355 and NIH P01CA217959 (KS and WAW) and P30CA082103 (WCG and WAW). Alex's Lemonade Stand, K08NS079485, DOD W81XWH-15-1-0166 (WCG), and the Intramural Research Programs of the National Center for Advancing Translational Sciences, National Institutes of Health.

☆☆ Conflicts of interest: KS has funding from Novartis Institute of Biomedical Research and consults for and has stock options in Auron Therapeutics and has served as an advisor for Kronos Bio. WAW has ownership interest in Auron Therapeutics, Nalo Therapeutics, and StemSynergy Therapeutics. JEB is a shareholder and employee of Novartis AG. WCG has ownership interest in Nalo Therapeutics and Revolution Medicines. NNS has interest in Revolution Medicines. The remaining authors declare no potential conflicts of interest.

Received 6 February 2021; received in revised form 3 May 2021; accepted 5 May 2021

© 2021 The Authors. Published by Elsevier Inc. This is an open access article under the CC BY-NC-ND license (http://creativecommons.org/licenses/by-nc-nd/4.0/)
https://doi.org/10.1016/j.neo.2021.05.003

TP53 restored, with marked tumor shrinkage and apoptosis induction in response to combination JQ1+Alisertib. BETi+AURKAi in *MYCN*-amplified NBL, particularly in the context of functional *TP53*, provided anti-tumor benefits in preclinical models. This combination should be studied more closely in a pediatric clinical trial.

Neoplasia (2021) 23, 624–633

Keywords: Neuroblastoma, MYCN, TP53, Synergy, Apoptosis

Introduction

Neuroblastoma (NBL) is the most common extracranial tumor of childhood, with greater than 650 children diagnosed each year in the United States [1]. While outcomes are heterogeneous, ranging from spontaneous remissions to a highly malignant, systemic illness, children with high-risk disease often have tumors with *MYCN*-amplification [2]. *MYCN* is a member of the MYC gene family (whose other members are *MYC* and *MYCL*) and encodes N-myc protein, a transcription factor with a basic helix-loop-helix-leucine zipper domain. Similar to *MYC* (among the most frequently amplified oncogenes in all cancers), *MYCN* is amplified in NBL and is also amplified/overexpressed in medulloblastoma, atypical teratoid rhabdoid tumors, neuro-endocrine prostate and lung cancer [3-6]. In NBL, *MYCN* amplification indicates aggressive disease and portends a poor prognosis [7,8]. Despite knowledge of these critical oncogenes for decades, there still are no direct inhibitors or degraders of MYC or N-myc.

Levels of N-myc are tightly controlled at the level of protein stability, with sequential phosphorylation by Cyclin B1/CDK1 and GSK3β leading to Fbxw7-mediated ubiquitination and subsequent proteasomal degradation [9]. In 2009, Otto *et* al. identified a direct interaction between the serine/threonine kinase Aurora kinase A (AURKA)and N-myc in NBL that protected it from proteasomal degradation [10]. AURKA was subsequently also found to similarly protect MYC in hepatocellular cancer models[11]. AURKA has been of interest as a cancer target for more than 20 years, as it is a cell cycle regulator that controls chromosomal segregation at mitosis and is amplified in various cancers [12]. MLN8237/Alisertib is an AURKA-specific inhibitor, with greater than 200-fold specificity for AURKA over AURKB (enzymatic AURKA IC_{50}: 1.2 nM, AURKB IC_{50} 396.5 nM, and cell-based IC_{50}: AURKA 6.7 nM and AURKB 1534 nM) [13]. Alisertib was developed to overcome the dose-limiting somnolence effects of its benzodiazepine predecessor MLN8054 [14,15]. While several small molecule inhibitors of AURKA have not been shown to affect N-myc levels, Alisertib has been shown to partially alter the conformation of AURKA, shifting the N-myc-AURKA binding equilibrium, and leading to some decrease in N-myc levels [16]. Alisertib also prolonged survival of a TH-*MYCN* NBL mouse model with loss of N-myc in the tumors [16]. Alisertib has been evaluated in multiple clinical trials in both adult and pediatric cancers [17-22]. In combination in pre-clinical models, it has been reported to be additive or synergistic with multiple agents, including vincristine [23], vorinostat [24], dexamethasone or bortezomib [25], cytarabine [26], and venetoclax [27]. Relevant to NBL, Alisertib added to the backbone of irinotecan+temozolomide improved survival of *in vivo* models and slowed tumor growth more than Alisertib alone or irinotecan+ temozolomide [28]. These results motivated a phase I trial combining Alisertib with irinotecan and temozolomide for patients with relapsed or refractory NBL, with a 31.8% overall response rate across all doses, but a 50% overall response rate at the Alisertib maximum tolerated dose (MTD) and two-year progression-free survival of 52.4% [29].

To improve on the anti-N-myc effects of MLN8237, we previously synthesized and characterized the binding of an AURKA conformation disrupting drug (CD532) that more efficiently disrupts interactions between AURKA and N-myc [30]. Marked N-myc loss was observed with 24 hours of CD532 treatment *in vitro*, and CD532 treatment of a NBL xenograft confirmed N-myc loss [30]. Recently LY3295668, another AURKA inhibitor (AURKAi), showed similar phenotypic effects to Alisertib in preclinical cancer models and now is being assessed in children with relapsed/refractory NBL [NCT04106219] [31]. Its specific effects on *MYCN* have not yet been reported, but together these data suggest that clinically relevant AURKAi can have a N-myc-destabilizing effect.

JQ1[32] and other BET bromodomain inhibitors (BETi) suppress the transcription of multiple genes (including *MYCN)* and downregulated *MYC/N*'s associated gene signatures in NBL and *MYC*-driven medulloblastoma [33-35]. This *MYCN* transcriptional downregulation was associated with G1 arrest, apoptosis induction, and, in multiple *in vivo* mouse models, prolongation of survival and delayed NBL progression [33,34]. Broadly BETi have been efficacious as single agents in many pre-clinical cancer models and are synergistic with many agents (reviewed in 36). However, clinical evaluation of single agent BETi have shown limited efficacy in adult patients with a variety of malignancies 37, perhaps due to dose-limiting side effects such as thrombocytopenia. This suggests combination therapy may be needed to minimize toxicities and to maintain durable responses. Pre-clinical determination of which combination partner is most synergistic in a given cancer is needed to guide optimal clinical trial assessments.

Two studies assessing the effect of BETi+AURKAi have recently reported efficacy in NBL and MYCN-elevated glioblastoma (GBM) models [38,39]. Felgenhauer *et* al. assessed the synergy between the BETi IBET151+Alisertib *in vitro,* and they observed the combination prolonged survival in both *MYCN*-amplified and non-amplified cell line xenograft NBL models. Čančer *et* al. demonstrated that JQ1-sensitive GBM cells had high *MYCN* expression, granting them more sensitivity to the JQ1+Alisertib combination. Taken together, these two studies suggest that the combination of Alisertib and JQ1 could be efficacious in other MYCN-driven tumors, in particular NBL, and prompted us to investigate further. Here we report that in *MYCN*-amplified NBL cell lines, the AURKAi class was among the most synergistic across all drug classes in reanalysis of our BETi combination screening of the Mechanism Interrogation PlatE (MIPE) drug library [40]. After confirming synergy of multiple agents of both drug classes, we found that MYCN was rapidly and sustainably downregulated more with JQ1+Alisertib combination treatment than either single agent. This prominently correlated with an induction of apoptosis. We extended these findings to *MYCN*-amplified, *TP53*-wild type cell lines and also showed that the combination of BETi +AURKAi suppressed tumor growth and prolonged survival *in vivo.* This was most pronounced in a highly aggressive, *MYCN*-driven genetically engineered model, in which functional *TP53* tripled survival in the combination-treated mice, which correlated with increased apoptotic markers. Therefore, the combination of BETi+AURKAi

targets the prototypical driver of aggressive NBL, has relevance regardless of *TP53* status, and lays the foundation for a clinical trial for patients with NBL.

Materials and Methods

Cell culture

All cell lines were obtained from ATCC and grown in their recommended cell culture medium: SK-N-BE(2)C, NGP, and Lan-1 were cultured in DMEM, while IMR-32 and Lan-5 were grown in RPMI-1640. All media was supplemented with 10% FBS and 1% Penicillin/Streptomycin and grown at 37°C in 5% CO_2. All cell lines were tested for mycoplasma contamination prior to experiments and authenticated by STR analysis at least annually. All cell lines were allowed to adhere for one day (two days for IMR-32) before they were treated with JQ1 (kind gift from Dr. Jun Qi) and/or Alisertib (Selleckchem, Cat# S1133) as experiments indicated.

TP53 CRISPR NGP cell line

NGP cells were transfected with sgRNAs targeting TP53. Briefly, we designed a pair of CRISPR guides to delete exon 5 so as to knock out full-length p53 and most of the p53 isoforms. Guide sequences (gRNAL1: 5' – tgactttcaactctgtctcc. gRNAR2: 5' – ggctggagagacgacagggc) were cloned into the px458 vector (Addgene, #48138), which were then electroporated into NGP cells. GFP+ cells were sorted and plated to isolate single clones. Candidate KO clones were screened by genomic PCR to confirm exon deletion and further verified by western blotting.

Cell viability and follow up synergy studies

All viability experiments were performed at least two times to ensure reproducibility with representative data shown. Cells were seeded onto 384-well tissue culture treated plates at a density of 12,500 cells/50 µL/well. The next day, compounds in DMSO (or DMSO-only control) were added to all wells using the HP D300 Digital Dispenser. Five to six concentrations were chosen to encompass the IC_{50} for each agent in the specific cell line used (previously determined). Compounds were added singly or in combination to the wells, allowing for quadruplicate of each dose pairing or single agent concentration. The entire plate was then DMSO-normalized for the highest DMSO volume added, not to exceed 0.02%/media/well. After 3-days of treatment, cells were analyzed for cell viability, utilizing the ATP luminescent assay kit (PerkinElmer) following manufacturer's instructions. The DMSO average for each plate was calculated, along with the standard deviation which had to be $\leq$10% standard error to be considered an interpretable experiment. Each well was then normalized to the DMSO average, and the single agent curves were plotted to confirm the doses selected did encompass the IC_{50}. Drug-induced death was calculated as 1-viability for each dose combination and entered into Calcusyn (Biosoft) to determine the normalized isobolograms, combination indices, and fraction affected for each drug-pairing, using the Chou-Talalay method of synergy calculations. Results were plotted in GraphPad Prism to illustrate the normalized isobolgram data generated from Calcusyn. For the NGP TP53 CRISPR drug combination testing, NGP parental and ΔTP53 cells were plated, and the next day a fixed active dose of JQ1 with various doses of Alisertib were added in triplicate. After 3-days of treatment, cells were analyzed for cell viability, utilizing the ATP luminescent assay kit. Results were plotted as bar graphs of various Alisertib doses comparing parental vs. ΔTP53 in GraphPad Prism.

Immunoblotting

All cell line immunblots were repeated at least one independent time with fresh cells, with representative blots shown. Cell lines were seeded at a density of 1×10^6 cells per 10cm plate. Cells were treated and collected after 6, 12, 24 and 48 hours with either JQ1 (500nM), Alisertib (100nM), or in combination. Cells treated to test the combination of JQ1+MK5108 were treated with 300nM MK5108 for 24 hours. Cells were lysed using RIPA lysis buffer and protease inhibitor (Halt Protease Inhibitor Cocktail), then the supernatant was collected. 10ug of protein were separated by SDS-PAGE, transferred to nitrocellulose membranes using the Trans-Blot Turbo System (Bio-Rad). After blocking in 5% milk/TBST, the members were probed overnight at 4°C with the following antibodies: MYCN (Santa Cruz Biotechnologies, sc-56729, or Abcam, ab16898), PARP (CST, 9542S), cleaved Parp (CST, 9541), Vinculin (Santa Cruz Biotechnologies, sc-25336), GAPDH-HRP (Proteintech, HRP-60004). After secondary antibody incubation with either anti-rabbit or anti-mouse IgG conjugated with horseradish peroxidase in 5% milk/TBST. Proteins were detected using ECL and imaged.

Mouse tumors (n = 2 from each treatment condition) were lysed in an NP-40-based lysis buffer (in house formulation) supplemented with fresh protease inhibitors (Sigma P8340). The samples were then sonicated on ice, centrifuged and the supernatant was collected. 20ug of protein was separated on an SDS-PAGE gel, followed by transfer to a nitrocellulose membrane as above. Membranes were blocked and incubated in 5% Milk/TBST, followed by overnight incubation at 4 °C in 0.5% Milk/TBST with the following antibodies: GAPDH (Millipore, MAB374) and cleaved caspase 3 (CST, 9661). After secondary antibody incubation with either anti-rabbit (for cleaved caspase 3) or anti-mouse IgG (for GAPDH) conjugated with horseradish peroxidase in 0.5% milk/TBST. Proteins were detected using ECL and imaged. Quantification of the protein bands was performed using Biorad's imaging analysis program, ImageLab.

RNA extraction and reverse transcriptase quantitative PCR (RT-qPCR)

All RT-qPCRs were repeated at least one separate time on freshly treated cells to confirm results with representative data shown. After 6 or 24 hours of drug treatment, cells were collected and counted with trypan blue. Equal cell numbers were harvested from all treatment conditions for RNA extraction ("cell count normalization"). RNA was extracted from cells using the Qiagen RNeasy Extraction Kit (74104), and cDNA was transcribed utilizing SuperScript Vilo (Invitrogen 11754-050). qPCR Taqman probes *MYCN, GAPDH* were obtained from Applied Biosystems. And qPCR was run on the 7500-Fast Real-Time PCR System (Applied Biosystems). Data was collected in technical triplicates and plotted as fold change using the ΔΔCt method compared to the vehicle control condition using GAPDH as the contro. Results were plotted in GraphPad Prism with standard error of the mean.

Flow cytometry

For both apoptosis and cell cycle measurements, all experiments were repeated at least once on freshly treated cells to confirm similar findings with representative data shown in the figures. Flowjo was used to analyze all samples after gating out for doublets. Results were plotted in GraphPad Prism as a mean+standard error of biologic triplicates of each treatment condition. For apoptosis determinations, cells were centrifuged after trypsinization and all but ~300-400uL media was aspirated. Equal volume of Annexin V buffer (10 mM HEPES pH 7.4, 140 mM NaCl, 2.5 mM $CaCl_2$–sterile filtered) containing 1 drop of DAPI solution (Invitrogen, NucBlue Fixed Cell Stain ReadyProbes reagent, R37606) per 1 mL buffer and 1:100 dilution of Annexin V-Alexa Fluor 488 antibody (Invitrogen, A13201) was added to each tube. All samples were analyzed on the BD LSRII. Early and late apoptotic cells (defined as Annexin V+) from each drug treatment condition were summed, averaged, and plotted.

For cell cycle analysis, cells were harvested and counted for equal numbers prior to a 1mL ice-cold PBS rinse. After the PBS rinse, cells were then resuspended in PBS and added dropwise to ice-cold 70% ethanol in a 1:10 dilution of cells:ethanol solution with vortexting. Cells were fixed overnight in -20deg C. The next day after centrifugation at 500g x10 minutes at 4deg C, the solution was removed and cells were resuspended in 3ml ice-cold PBS. After another centrifugation at 500g x10 minutes at 4deg C, PBS was removed, and 500uL PI staining solution was added to each tube: (0.02mg/ml RNase, 0.02mg/ml propidium iodide, 0.1% triton X in PBS). After a 20-minute incubation at 37deg C, tubes were placed on ice and read within 48 hours on the BD CantoII. The cell cycle analysis tool of Flowjo was used to determine % of cells in each phase and results were averaged and plotted in GraphPadPrism.

Caspase-Glo

Cells were seeded at 20,000 cells/well into a 96-well plate in triplicate with drug or drug combination added to each well the following day. After 24 hours of treatment, plates were centrifuged, 100uL of media removed, and then 100uL of room-temperature caspase-glo reagent added (Caspase-Glo 3/7 Assay, Promega Corporation). After brief shaking and another centrifugation, the plate was incubated for 1 hour at room temperature protected from light before reading luminescence signal on the Infinite M1000 Pro Plate Reader. Luminescent signal was normalized as a ratio to the DMSO signal and plotted in GraphPad Prism.

In vivo *studies*

THMYCN P53 pathway mutant mice (THp53ER) were generated as previously described [41]. THp53ER tumors were allografted subcutaneously into 4-6 week-old 129 × 1/SvJ mice (Jackson Laboratories, Bar Harbor, ME, Stock number 000691). Once tumors reached 300-500 mm^3, mice were randomly enrolled into 8 treatment groups (n = 5/treatment group). Mice were treated with 50 mg/kg JQ1 intraperitoneal injection (kind gift from Dr. Jun Qi) and/or 30 mg/kg Alisertib by oral gavage (OG, MedChemExpress Co, HY-10971) and/or 40 mg/kg Tamoxifen OG (Sigma Aldrich, T5648), or vehicle daily for 5 days per week, with 1mL subcutaneous normal saline (0.9%) supplemented during treatment days. JQ1, Alisertib, and Tamoxifen were formulated in 10% 2-hydroxypropyl-β-cyclodextrin (Spectrum Chemical, H2690), 10% 2-hydroxypropyl-β-cyclodextrin/1% Sodium bicarbonate, or peanut oil, respectively. Mice were treated for a total of 24 days. Tumor volume was determined by caliper measurements three times per week and calculated using the following formula: 1/2(Length × Width [2]). Mice were euthanized when tumors reached 2 cm in diameter. Survival was determined using a Kaplan-Meier analysis in GraphPad Prism and compared by a log-rank Mantel-Cox analysis. In a separate experiment, mice were euthanized, and tumors were harvested 1 hour after their 2nd day of treatment for pharmacodynamic analysis (n = 3/treatment group). All animal studies were conducted according to approved protocols by the Animal Care and Use Committee of the University of California San Francisco (UCSF IACUC).

Tumor immunohistochemistry

Formalin fixed paraffin embedded tumor tissue from mice treated for 2 days were sliced manually with a manual microtome (Leica, RM2155) to 5 μm depth. H&E staining was preformed using Gill's II Hematoxylin (Sigma-Aldrich, GHS216) and Eosin Y (VWR, 95057-848). For IHC, slides were stained with cleaved caspase 3 antibody (Cell Signaling Technology, 9661), and counterstained with Gill's II hematoxylin. Slides were visualized using a Leica DMi8 automated microscope and also scanned by HistoWiz for low-power visualization.

Statistical methods

Synergy was calculated using the Chou-Talalay method within the Calcusyn software. Combination indices (CIs) were reported by Calcusyn for all dose combinations tested—the median value of all CIs was reported. For RTqPCR, Annexin V detection, and CaspaseGlo, all treatment conditions were compared to DMSO (asterisks shown over individual bars) and single agent to combination all by one-way analysis of variance (ANOVA) with Bonferroni post-tests with multiple comparisons. For cell cycle analysis, statistical analysis was two-way ANOVA with Bonferroni post-tests with multiple comparisons. Survival analysis was calculated for significance using a log-rank Mantel-Cox test. All statistical analyses were conducted with Graphpad Prism 5 (GraphPad Software Inc, La Jolla, CA) with a p-value cutoff of < 0.05 was considered statistically significant for all experiments.

Results

Aurora kinase inhibitors are among the most synergistic of all drug classes in combination with BETi in MYCN*-amplified NBL cell lines*

In collaboration with the National Center for Advancing Translational Sciences, we previously performed a viability matrix combination screen of their MIPE library of ~1900 oncology-focused compounds [42] to identify anti-NBL, synergistic combinations with two BETi (JQ1 and IBET151) in two *MYCN*-amplified, *TP53* mutant NBL cell lines (Lan-1 and SK-N-BE(2)C [hereafter referred to as BE(2)C])[40]. In general, an interpretable, matrix-level quality control measure mQC (described in reference 43), confirmed confidence in the results, with the vast majority of drug combinations in both cell lines rating "good," (>95% of BE(2)C combinations and 80% of Lan-1 combinations). Over half of all drugs in the MIPE library demonstrated some degree of synergy with the BETi, as demonstrated by a delta Bliss Sum Negative (DBSumNeg) value that was < 0 based on the Bliss Independence model of synergy determination [44]. Overall the most synergistic classes of drugs were those affecting cell cycle, including cyclin-dependent kinase inhibitors and PI3K/IGF1R inhibitors as we previously reported [40]. Strikingly, reanalysis of our data uncovered that both *MYCN*-amplified cell lines also demonstrated a marked sensitivity to the combination of BETi with another class of cell cycle regulators: aurora kinase inhibitors, including AURKAi (Fig. 1A).

One of the most synergistic AURKAi in both cell lines was MK-5108. Specific matrix combination evaluation of JQ1+MK-5108 in both cell lines confirmed diminished cell viability comparing combinations to either agent alone in multiple dose ranges (6 × 6 comparison, Fig. 1B). This specific class synergy was confirmed across a wider-range (10 × 10) of doses for several AURKAi and JQ1 and IBET-151 (Supplementary Fig. 1A and 1B). More broadly, the viability and delta Bliss (ΔBliss) matrices for all the AURKAi (21 in the entire library) + the two BETi confirmed the sensitivity of these two *MYCN*-amplified cell lines to this combination (Fig. 1C, Supplementary Fig. 1A and 1B). Overall, in BE(2)C cells, seven of the total 21 aurora kinase inhibitors had a negative DBSumNeg in the lowest quartile of all MIPE drugs, while 15 aurora kinase inhibitors in Lan-1 had a DBSumNeg value in the lowest quartile of the 1900 compound library. Of these lowest quartile aurora kinase inhibitors, 71% (n = 5/7) and 87% (n = 13/15) had AURKAi specific activity in the two respective cell lines. While the two cell lines' sensitivity to the BETi combination may be due to known effects of Aurora B kinase inhibition [45-47], we chose to further explore the mechanism of synergy underlying BET inhibition in combination with more specific AURKA inhibition, since both were independently reported to downregulate MYCN and are currently in clinical trials.

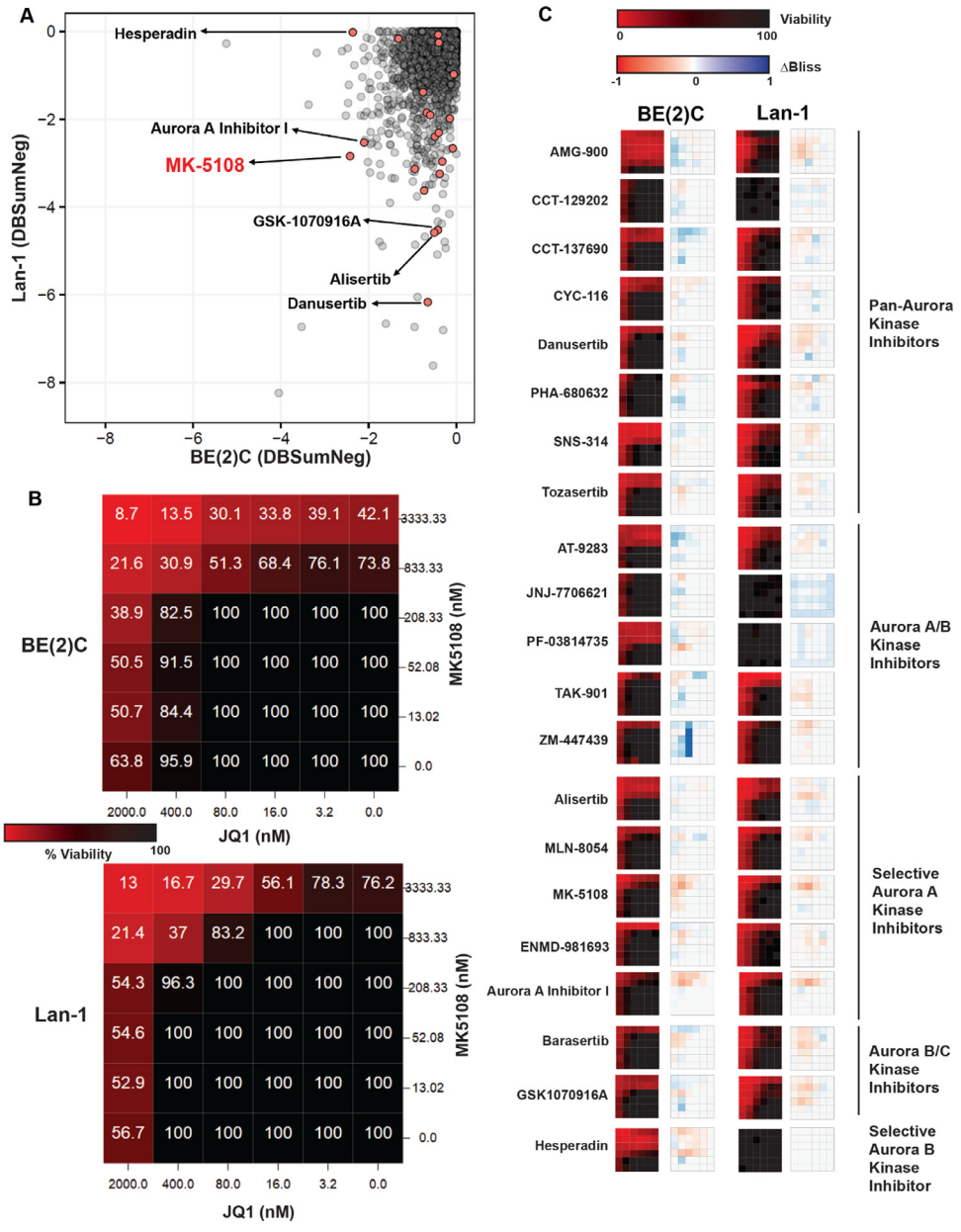

Fig. 1. High-Throughput Screen of *MYCN*-Amplified Neuroblastoma Identifies Synergy with Inhibitors of aurora A kinase (AURKA) and BET. (A) Cytotoxicity screen of two *MYCN*-amplified neuroblastoma (NBL) cell lines (BE(2)C, Lan-1) treated with the BET inhibitor JQ1 combined with NCATS' MIPE library for 72 hours as previously reported in ref [17]. Combinations with aurora kinase inhibitors (AURKi) are highlighted in red. The delta Bliss Sum Negative (DBSumNeg) values <0 (indicating synergy) for each drug pairing in each cell line is shown. (B) Heat map of BE(2)C and Lan-1 cell viability when treated with increasing concentrations of JQ1 and MK-5108, the most synergistic AURKi. Black indicates 100% viable cells; shades of red indicate remaining live cells. (C) 6 × 6 heat maps of viability effects (left; scale same as Figure 1B) and delta Bliss synergy (right) with treatment of JQ1 combined with each AURKi in the MIPE library in each NBL cell line. Blue indicates synergy as determined by the Bliss Independence model of synergy determination; red indicates antagonism.

BETi and AURKAi have synergistic, antiproliferative effects in MYCN*-amplified NBL cell lines*

We validated the combination of Alisertib with JQ1 in the two *MYCN*-amplified cell lines BE(2)C and Lan-1 across 6-7 concentrations for each agent (Fig. 2A). We confirmed that across most of the concentrations tested, the two agents were at least additive and more often synergistic with median combination indices (CI) of 0.666 for BE(2)C and 0.537 for Lan-1 (Fig. 2F). Additionally, we observed the majority of concentration pairings had a CI <1 (Fig. 2B) and almost all the concentrations significantly decreased the viability of both cell lines (Supplementary Fig. 2A). We then expanded our studies to several other clinical BETi: IBET (Fig. 2C) and OTX-015 (Fig. 2D) and confirmed the class-wide synergy with Alisertib. MK-5108, the most synergistic AURKAi in both cell lines in the MIPE drug screen, was also confirmed to be synergistic with JQ1 in our hands (Fig. 2E), though less so with IBET or OTX-015 (Supplementary Fig. 2B and 2C). Across the dose pairings, the two classes of inhibitors had median CIs that confirmed mild to moderate synergy in *MYCN*-amplified NBL (Fig. 2F).

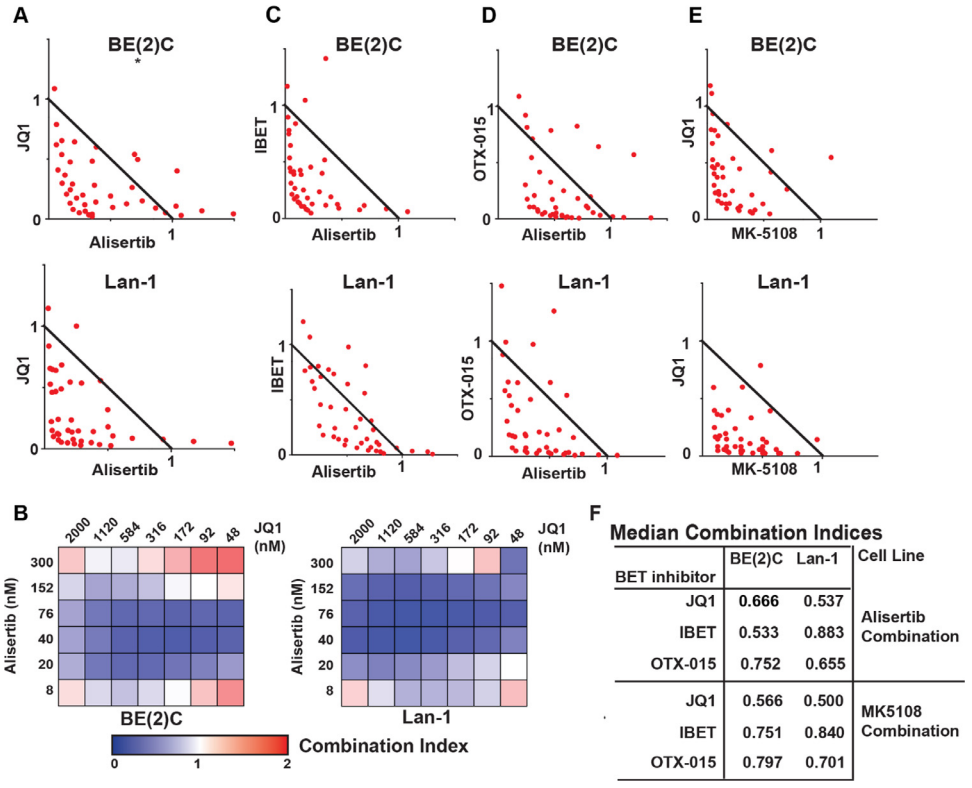

Fig. 2. Synergistic Combination of BET inhibitor (BETi) class with AURKAi class in *MYCN*-Amplified Neuroblastoma. (A) Normalized isobolograms of synergy calculations of JQ1 + the AURKAi Alisertib in BE(2)C (top) and Lan-1 (bottom) (72 hours of treatment, n=4 replicates for each dose pairing).* indicates dose pairing out of range of graphical depiction. Calcusyn used to calculated synergy. (B) Heat map of the combination indices (CI) for each dose combination, with <1 (shades of blue) indicating synergy and >1 (shades of red) indicating antagonism. (C-E) Normalized isobolograms of various BETi (IBET, C; OTX-015, D) + Alisertib, or JQ1+ the AURKAi MK-5108 (E) in both *MYCN*-amplified cell lines. (F) Median combination indices of all BETi+AURKAi in both *MYCN*-amplified cell lines.

BETi and AURKAi combination synergistically inhibits MYCN

We then sought to better understand the effects of BETi and AURKAi in combination on MYCN. Based on published mechanisms, we would anticipate BETi to decrease the level of *MYCN* mRNA and Alisertib to decrease the level of N-myc protein. To confirm this mechanism, we first assessed expression changes in the *MYCN* gene by RT-qPCR. Because MYC and N-myc are global transcriptional amplifiers [48,49], we performed cell-count normalized RT-qPCR of the *MYCN* transcript after 6 and 24 hours of compound treatment and observed JQ1 produced a rapid and sustained decrease in *MYCN* transcription in NBL cells, as previously reported [33] (Fig. 3A). There was no further suppression of *MYCN* transcription in cells which received the combination of JQ1+Alisertib compared to JQ1 alone. We did not observe any effect of Alisertib on *MYCN* mRNA levels in BE(2)C cells; however Lan-1 cells exhibited decreased *MYCN* expression with Alisertib treatment alone, but the combination did not further decrease its expression. We next evaluated the effects of the combination on N-myc protein levels and observed no effect on N-Myc at 6 hours. But at 24 and 48 hours of treatment, there was sustained, combinatorial synergy of the two agents in both cell lines with near complete loss of N-myc at these times (Fig. 3B). Similar findings were seen with 24-hour treatment of JQ1+MK-5108 in these two cell lines (Supplementary Fig. 3A).

To determine the relative contribution of proteasomal degradation underlying this synergistic MYCN effect of the combination, we then treated BE(2)C or Lan-1 cells for the same duration, with the addition of the proteasome inhibitor MG-132 for the last 4 hours of the 24-hour BETi/AURKAi treatments. For all conditions, addition of MG-132 restored levels of N-myc (Fig. 3C). However, this restoration was incomplete in the JQ1- or combination-treated cells, consistent with BETi+AURKAi synergizing to downregulate MYCN via multiple avenues, even without proteasomal degradation.

JQ1+Alisertib combination blocks NBL cells in G2 and markedly induces apoptosis

To explore the specific phenotypic effects causing the synergy seen with these two inhibitors on *MYCN*-amplified cell lines, we assessed cell cycle alterations of the treatment combination. BETi are known to arrest cells in G1 (at least in part due to their downregulatory effects on MYC), and AURKAi potently arrest cells in G2 [30,33]. Twenty-four hour treatment of both BE(2)C and Lan-1 cells with single agent JQ1, Alisertib, or the combination confirmed diminished S-phase in nearly all treatment conditions (gray bars, Fig. 3D). We observed increased G1 arrest with JQ1 treatment and G2 arrest with Alisertib, while the combination resulted in a predominant G2 arrest. As Alisertib directly impacts cell cycle while, in contrast, JQ1 exerts transcriptional effects that indirectly alter the cell cycle, our findings likely reflect that once the cells are arrested in one phase of the cell cycle, this arrest is likely to prevent progression to another phase.

We then evaluated the likelihood of the combination inducing apoptosis: both cell lines treated with the JQ1+Alisertib combination demonstrated significant annexin V expression than single agents alone (Fig. 3E). These findings were overall confirmed both by caspase 3/7 activation and detection of cleaved PARP (Fig. 3F and 3G).

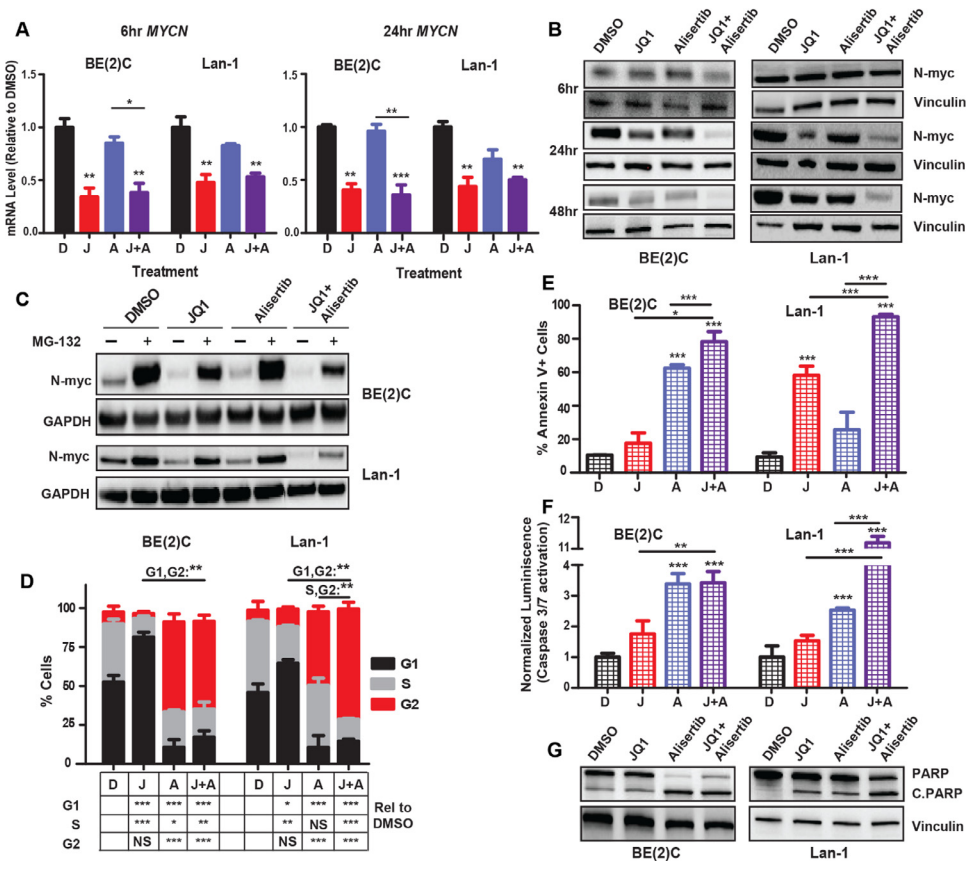

Fig. 3. Multiple Mechanisms Underlying BETi + AURKAi Synergy in *MYCN*-Amplified NBL. n=3 technical replicates for each experiment, with each experiment run at least two independent times, and representative results shown. (A) Effect of treatment with JQ1 (500nM), Alisertib (100nM), or combination on cell-count normalized *MYCN* mRNA after 6 hours and 24 hours of treatment. D= DMSO, J= JQ1, A=Alisertib, J+A= JQ1+Alisertib. All samples normalized to GAPDH expression by ΔΔCt method. Conditions were compared to DMSO (asterisks shown over individual bars) and single agent to combination (lines denoting the two conditions compared), all by one-way ANOVA with Bonferroni post-tests with multiple comparisons. (B) JQ1+Alisertib treatment effects on N-myc over time, as indicated. (C) N-myc loss in BETi+AURKAi combination with or without the proteasomal inhibitor MG-132 treatment (5 μM) for the last 4 hours of a 24-hour treatment. (D) Effect of JQ1+Alisertib on the cell cycle after 24 hours of treatment. Samples were compared by two-way ANOVA with Bonferroni post-tests with multiple comparisons. Statistics between single agent and combination represented above the bars, with all phases of cell cycle changes relative to DMSO shown in the table below. (E-G) Detection of apoptosis in *MYCN*-amplified NBL cells treated with JQ1, Alisertib, or combination when measured by (E) Annexin-V expression (48 hours treatment), (F) Caspase 3/7 activation (as measured by luminescence by Caspase-Glo, 24 hours treatment), and (G) PARP cleavage (c. PARP=cleaved PARP, 12 hours treatment). All treatment conditions were compared to DMSO and each single agent to combination by one-way ANOVA with Bonferroni post-tests with multiple comparisons. For all comparisons, * = $p < 0.05$, ** = $p < 0.01$, *** = $p < 0.001$.

Functional TP53 confers sensitivity to AURKAi+BETi treatment

While our initial studies were conducted in *MYCN*-amplified, *TP53*-mutant cell lines, most NBLs initially retain wild-type germline *TP53* [50]. We therefore sought to evaluate the efficacy of this combination in *MYCN*-amplified, *TP53*-wild type cell lines for potential broader translational applicability. Also, while p53 function is linked to chemotherapy sensitivity (and its loss contributes to multi-drug resistance) [51,52], a recent publication indicated JQ1 downregulated MDM2, allowing p53 to accumulate and induce apoptosis [53]. Specific evaluation of two *TP53*-wild type, *MYCN*-amplified NBL cell lines confirmed synergistic anti-proliferative effects of JQ1+Alisertib with similar median combination indices than those seen in the *TP53*-mutant, *MYCN*-amplified cell lines (Fig. 4A). N-myc loss, induction of apoptosis, and G2 arrest were also observed with the combination in the *TP53*-wild type cells (Fig. 4B, Supplementary Fig. 4A-4D). To determine if the presence of functional p53 correlated to heightened sensitivity to the BETi+AURKAi combination, we generated an isogenic *TP53* knockout clone of the *MYCN*-amplified (but JQ1-resistant and MDM2-amplified) NBL cell line NGP. After confirming knockout of *TP53* compared to parental NGP cell line (Supplementary Fig. 4E), we treated both parental and *TP53*-KO NGP cell lines with a fixed, effective concentration of JQ1 and multiple concentrations of Alisertib. The *TP53*-KO NGP cells were generally more resistant to single agent JQ1, and while the addition of several effective concentrations of Alisertib increased the non-viable cells in both cell lines, the *TP53*-KO cells remained less sensitive to the combination than the parental NGP cell lines (Fig. 4C), suggesting *TP53*-mutant cells may generally have diminished sensitivity to BETi+AURKAi compared to *TP53*-WT cells.

Increased apoptosis prolongs the survival benefit of BETi+AURKAi observed in TP53*-restored* in vivo *models*

Based on the above results, and previously published data of the aggressive TH-MYCN, *TP53*-inducible mouse model, we evaluated the drug

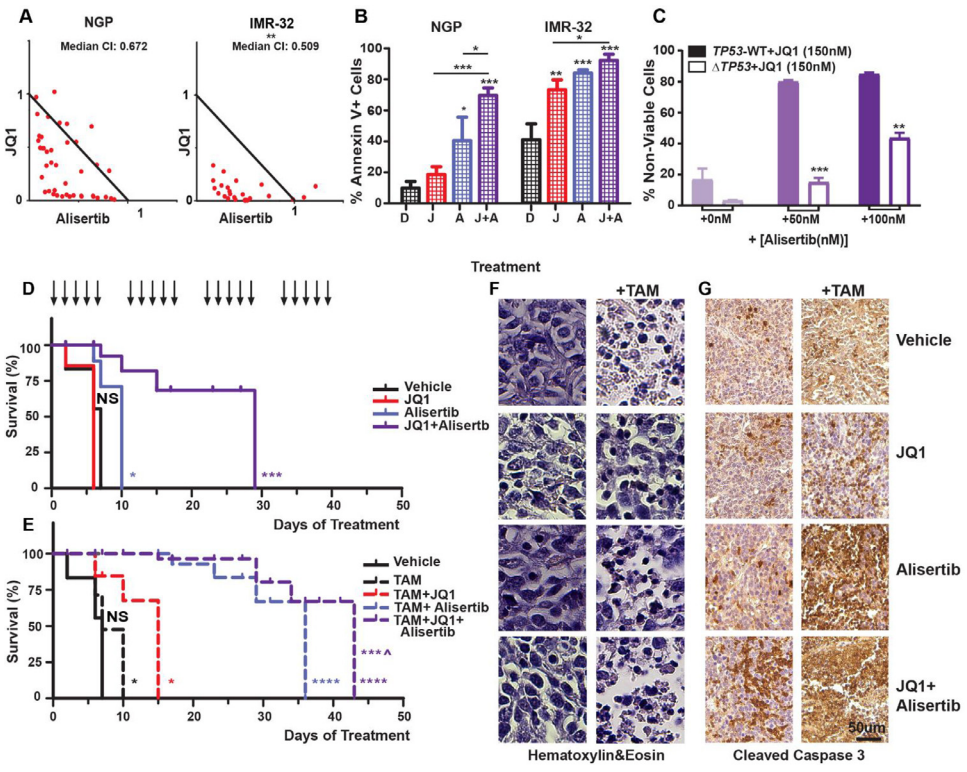

Fig. 4. BETi + AURKAi Combination Is Active in *MYCN*-Amplified, *TP53*-wild type NBL. (A) Normalized isobolograms of JQ1+Alisertib treated *MYCN*-amplified, *TP53*-wild type NGP or IMR-32 cells (72 hours treatment, n=4 replicates for each dose pairing). * indicates dose pairing out of range of graphical depiction. (B) Degree of apoptosis (as measured by Annexin V+) induced by single agent or combination treatment of NGP and IMR32 cells (48 hours treatment). D= DMSO, J= JQ1, A=Alisertib, J+A= JQ1+Alisertib. All treatment conditions were compared to DMSO and each single agent to combination by one-way ANOVA with Bonferroni post-tests with multiple comparisons. (C) Percentage of non-viable cells detected in an isogenic NGP NBL cell line with *TP53*-wild-type or *TP53*-knockout by CRISPR/Cas9, treated with 0, 50, or 100 nM Alisertib added to a fixed JQ1 concentration of 150 nM. (72h of treatment, n=3 biologic replicates for each dose combination). Knockout cells were compared parental for each Alisertib concentration by student's t-test. (D, E) In a conditional TP53-restored model regulated by Tamoxifen (TAM, 40mg/kg oral gavage [OG]), survival effects of single agent (JQ1 50mg/kg intraperitoneal injection [IP], Alisertib 30mg/kg OG) or combination JQ1+Alisertib without TAM (D) or with TAM administration (E) (n=5 mice/treatment arm). Kaplan-Meier analysis was used to determine survival difference with log-rank (Mantel-Cox) statistical comparisons between each treatment arm and vehicle control (shown to the right of each curve). ***^=statistical significance of p<0.001 between JQ1+Alisertib of fig 4D and TAM+JQ1+Alisertib. (F,G) Representative tumor sections from mice treated for 2 days with JQ1, Alisertib, or combination +/- TAM with sections stained with Hematoxylin&Eosin (F) or for cleaved caspase 3 (G). For all comparisons, * = $p < 0.05$, ** = $p < 0.01$, *** = $p < 0.001$, **** = $p < 0.0001$.

combination in *in vivo* models in the presence and absence of functional p53 (Fig. 4D-4E). This model, reported by Yogev et al.[41], is a genetically engineered, MYCN-driven model that also has the endogenous *trp53* gene replaced with a knock-in allele (Trp53KI) encoding a 4-hydroxytamoxifen (4-OHT)–regulatable p53ERTAM fusion protein. In the presence of 4-OHT (a metabolite of tamoxifen, TAM), the hormone-binding domain of the estrogen receptor (ER) is released from its inhibitory conformation, and p53ERTAM translocates to the nucleus. Homozygous TH-MYCN transgenic mice are highly penetrant, developing tumors within 7 to 8 weeks of birth. In the absence of functional p53, single agent Alisertib or JQ1 had minimal benefit in suppressing tumor volume compared to vehicle alone (Supplementary Fig. 4F). Combining JQ1 and Alisertib led to 50% tumor regression within the first week of treatment. However, this was not sustained, and tumors eventually doubled in size until the mice were sacrificed. Solely restoring p53 function also had minimal benefit over vehicle or single agent alone, while addition of JQ1 delayed tumor growth by only a few days. However, when Alisertib was administered, there was more pronounced tumor growth inhibition. Furthermore, the two compounds in the setting of functional p53 had more sustained tumor shrinkage out to 28 days before resistance eventually developed when the agents were discontinued .

We also examined the survival benefit of these agents in this aggressive model (Fig. 4D-4E). While a similar lack of benefit with the single agents were seen with mice dying within 10 days of treatment initiation, the drug combination (in the *TP53* null context) prolonged survival by >20 days (Fig. 4D, purple line). Restoration of p53 again had minimal effect on its own, with JQ1 providing slight additional benefit (Fig. 4E, black- vs. red-dotted lines). Alisertib in the setting of functional p53 prolonged survival almost 30 days more than vehicle alone, and the JQ1+Alisertib drug combination with functional p53 prolonged survival nearly 36 more days than vehicle (Fig. 4E, blue- and purple-dotted line), and also significantly prolonged survival than the JQ1+Alisertib in the context of p53-null. We conclude that Alisertib cooperates with functional p53 and JQ1 for maximal survival benefit *in vivo*.

A subset of mice was treated for two days and then sacrificed, with tumors harvested for pharmacodynamic effects. Hematoxylin & Eosin staining demonstrated fewer cells and some pyknotic cells with JQ1+Alisertib treatment that was heightened with restored p53 (Fig. 4F). Staining for cleaved caspase 3 confirmed our *in vitro* findings with increased caspase 3 activation with Alisertib and strongest with JQ1+Alisertib that was heightened with functional p53 (Fig. 4G). These findings were also seen on low-power images of the tumor and cleaved caspase 3 western blot of

the tumors (Supplementary Fig. 4G-H). Together these data indicate that AURKAi favorably interact with functional p53 for anti-NBL effects which is driven by apoptosis induction, and that combining AURKAi with BETi provides synergistic anti-NBL benefit.

Discussion

We previously performed a screen to find BETi-synergistic agents in a library of nearly 2000 focused, cancer-active agents [40]. In our screen, various classes of cell cycle regulators were synergistic with BETi, confirming studies in other cancer models, including our work in MYC-driven medulloblastoma [54,55], and identified BETi resistance mechanisms in NBL [40]. In the current work, we focus on another highly synergistic class identified in this screen: BETi with AURKAi. AURKAi and BETi have previously been shown to downregulate N-myc protein and *MYCN* transcription respectively, and we hypothesized a double hit on MYCN as a mechanism for the observed synergy. Among the inhibitors we tested, the aurora kinase inhibitor most synergistic with BETi in both *MYCN*-amplified NBL cell lines was MK-5108, an AURKAi with >200-fold selectivity for AURKA over AURKB. In fact, other multiple AURKAi also synergized with BETi, supporting a class effect across AURKAi. We focused our experiments on Alisertib, which recently completed a phase II pediatric trial in patients with NBL, demonstrating benefit when given in combination with chemotherapy [20].

We observed synergistic, antiproliferative effects and downregulation of N-myc with Alisertib combined with various BETi by decreased *MYCN* mRNA by BETi and increasing degradation of N-myc protein through AURKAi. In addition to anti-N-myc effects, Alisertib induced cell cycle arrest in all our NBL cell lines. Ultimately, apoptosis was induced by the BETi+AURKAi combination in all cell lines tested, with the immediate apoptosis effectors PARP and caspase 3 upregulated *in vitro* and/or *in vivo*. Recently it was also shown that Alisertib+ IBET-151 has a beneficial effect in NBL, indicating effects are not limited to N-myc but also extend to MYC-expressing NBL [38]. In this study we show the potential importance of p53 status in NBL tumors treated with Alisertib or BETi monotherapy compared with the combination.

While deletion or mutation of *TP53* is common in NBL cell lines, *TP53* loss is significantly less common (but occasionally present) in NBL patient tumors at diagnosis and at relapse [56,57]. Cell cycle arrest and induction of apoptosis are the end effects of the combination of AURKAi and BETi in NBL cell lines and tumors. These were most prominently seen in p53 intact cell lines and in our *TP53*-restored, *MYCN*-driven mouse model which had striking prolongation of survival and decreased tumor burden with both Alisertib monotherapy (consistent with prior studies [58]), and enhanced by the addition of the BETi JQ1. In contrast, p53 loss conferred partial resistance of the *MYCN*-amplified tumors to Alisertib monotherapy while the combination of AURKAi + BETi was effective in both the presence and absence of functional p53. This suggests *TP53* status may be predictive of response to AURKAi therapy in NBL, that it may predict a future mechanism of emergent resistance to Alisertib in NBL, and that the combination of JQ1 and Alisertib could partially overcome this mechanism of resistance. In light of these findings, p53 status should be considered in the design of future NBL clinical trials with Alisertib or Alisertib plus BETi.

In conclusion, we demonstrate that combination of BET and AURKA inhibition has synergistic, anti-NBL effects in *MYCN*-amplified disease through loss of MYCN, blockade of the cell cycle, and induction of apoptosis in both p53 wild type and mutant NBL. While loss of p53 confers resistance to monotherapies, the combination further overcomes resistance to AURKAi or BETi monotherapy across models of p53 wild type and mutant NBL. These studies lay the preclinical foundation for the development of a clinical trial to evaluate this combination in children with *MYCN*-amplified NBL.

Acknowledgements

We thank Dr. Ronald Bernardi for his critical reading of the manuscript and thoughtful consultations. This project was supported by the Cytometry and Cell Sorting Core at Baylor College of Medicine (BCM) with funding from the NIH (NIAID P30AI036211, NCI P30CA125123, and NCRR S10RR024574) and the assistance of Joel M. Sederstrom. Support was also provided by the BCM Cell-Based Assay Screening Service Core at Baylor College of Medicine with funding from the NIH (P30 CA125123) and the expert assistance of Drs. Dan Liu and Jun Xu.

Supplementary materials

Supplementary material associated with this article can be found, in the online version, at doi:10.1016/j.neo.2021.05.003.

References

1 Howlader NNA, Krapcho M, Garshell J, Neyman N, Altekruse SF, Kosary CL, Yu M, Ruhl J, Tatalovich Z, Cho H, et al., editors. *SEER Cancer Statistics Review, 1975-2010*. Bethesda, MD: National Cancer Institute; 2013.

2 Kreissman SG, Seeger RC, Matthay KK, et al. Purged versus non-purged peripheral blood stem-cell transplantation for high-risk neuroblastoma (COG A3973): a randomised phase 3 trial. *Lancet Oncol* 2013;**14**:999–1008.

3 Aldosari N, Bigner SH, Burger PC, et al. MYCC and MYCN oncogene amplification in medulloblastoma. A fluorescence in situ hybridization study on paraffin sections from the Children's Oncology Group. *Arch Pathol Lab Med* 2002;**126**:540–4.

4 Johann PD, Erkek S, Zapatka M, et al. Atypical Teratoid/Rhabdoid Tumors Are Comprised of Three Epigenetic Subgroups with Distinct Enhancer Landscapes. *Cancer Cell* 2016;**29**:379–93.

5 Beltran H, Rickman DS, Park K, et al. Molecular characterization of neuroendocrine prostate cancer and identification of new drug targets. *Cancer Discov* 2011;**1**:487–95.

6 Chen C, Breslin MB, Lan MS. Sonic hedgehog signaling pathway promotes INSM1 transcription factor in neuroendocrine lung cancer. *Cell Signal* 2018;**46**:83–91.

7 Nesbit CE, Tersak JM, Prochownik EV. MYC oncogenes and human neoplastic disease. *Oncogene* 1999;**18**:3004–16.

8 Beroukhim R, Mermel CH, Porter D, et al. The landscape of somatic copy-number alteration across human cancers. *Nature* 2010;**463**:899–905.

9 Sjostrom SK, Finn G, Hahn WC, Rowitch DH, Kenney AM. The Cdk1 complex plays a prime role in regulating N-myc phosphorylation and turnover in neural precursors. *Dev Cell* 2005;**9**:327–38.

10 Otto T, Horn S, Brockmann M, et al. Stabilization of N-Myc is a critical function of Aurora A in human neuroblastoma. *Cancer Cell* 2009;**15**:67–78.

11 Dauch D, Rudalska R, Cossa G, et al. A MYC-aurora kinase A protein complex represents an actionable drug target in p53-altered liver cancer. *Nat Med* 2016;**22**:744–53.

12 Zhou H, Kuang J, Zhong L, et al. Tumour amplified kinase STK15/BTAK induces centrosome amplification, aneuploidy and transformation. *Nat Genet* 1998;**20**:189–93.

13 Manfredi MG, Ecsedy JA, Chakravarty A, et al. Characterization of Alisertib (MLN8237), an investigational small-molecule inhibitor of aurora A kinase using novel in vivo pharmacodynamic assays. *Clin Cancer Res* 2011;**17**:7614–24.

14 Macarulla T, Cervantes A, Elez E, et al. Phase I study of the selective Aurora A kinase inhibitor MLN8054 in patients with advanced solid tumors: safety, pharmacokinetics, and pharmacodynamics. *Mol Cancer Ther* 2010;**9**:2844–52.

15 Dees EC, Infante JR, Cohen RB, et al. Phase 1 study of MLN8054, a selective inhibitor of Aurora A kinase in patients with advanced solid tumors. *Cancer Chemother Pharmacol* 2011;**67**:945–54.

16 Brockmann M, Poon E, Berry T, et al. Small molecule inhibitors of aurora-a induce proteasomal degradation of N-myc in childhood neuroblastoma. *Cancer Cell* 2013;**24**:75–89.

17 Cervantes A, Elez E, Roda D, et al. Phase I pharmacokinetic/pharmacodynamic study of MLN8237, an investigational, oral, selective aurora a kinase inhibitor, in patients with advanced solid tumors. *Clin Cancer Res* 2012;**18**:4764–74.

18 Mosse YP, Lipsitz E, Fox E, et al. Pediatric phase I trial and pharmacokinetic study of MLN8237, an investigational oral selective small-molecule inhibitor of Aurora kinase A: a Children's Oncology Group Phase I Consortium study. *Clin Cancer Res* 2012;**18**:6058–64.

19 Mosse YP, Fox E, Teachey DT, et al. A Phase II Study of Alisertib in Children with Recurrent/Refractory Solid Tumors or Leukemia: Children's Oncology Group Phase I and Pilot Consortium (ADVL0921). *Clin Cancer Res* 2019;**25**:3229–38.

20 DuBois SG, Mosse YP, Fox E, et al. Phase II Trial of Alisertib in Combination with Irinotecan and Temozolomide for Patients with Relapsed or Refractory Neuroblastoma. *Clin Cancer Res* 2018;**24**:6142–9.

21 Matulonis UA, Sharma S, Ghamande S, et al. Phase II study of MLN8237 (alisertib), an investigational Aurora A kinase inhibitor, in patients with platinum-resistant or -refractory epithelial ovarian, fallopian tube, or primary peritoneal carcinoma. *Gynecol Oncol* 2012;**127**:63–9.

22 Melichar B, Adenis A, Lockhart AC, et al. Safety and activity of alisertib, an investigational aurora kinase A inhibitor, in patients with breast cancer, small-cell lung cancer, non-small-cell lung cancer, head and neck squamous-cell carcinoma, and gastro-oesophageal adenocarcinoma: a five-arm phase 2 study. *Lancet Oncol* 2015;**16**:395–405.

23 Mahadevan D, Stejskal A, Cooke LS, et al. Aurora A inhibitor (MLN8237) plus vincristine plus rituximab is synthetic lethal and a potential curative therapy in aggressive B-cell non-Hodgkin lymphoma. *Clin Cancer Res* 2012;**18**:2210–19.

24 Muscal JA, Scorsone KA, Zhang L, Ecsedy JA, Berg SL. Additive effects of vorinostat and MLN8237 in pediatric leukemia, medulloblastoma, and neuroblastoma cell lines. *Invest New Drugs* 2013;**31**:39–45.

25 Gorgun G, Calabrese E, Hideshima T, et al. A novel Aurora-A kinase inhibitor MLN8237 induces cytotoxicity and cell-cycle arrest in multiple myeloma. *Blood* 2010;**115**:5202–13.

26 Kelly KR, Nawrocki ST, Espitia CM, et al. Targeting Aurora A kinase activity with the investigational agent alisertib increases the efficacy of cytarabine through a FOXO-dependent mechanism. *Int J Cancer* 2012;**131**:2693–703.

27 Ham J, Costa C, Sano R, et al. Exploitation of the Apoptosis-Primed State of MYCN-Amplified Neuroblastoma to Develop a Potent and Specific Targeted Therapy Combination. *Cancer Cell* 2016;**29**:159–72.

28 Lipsitz EG, Nguyen V, Zhao H, Ecsedy J, Maris JM, Adamson PC, Mosse YP. Modeling MLN8237, an aurora kinase a inhibitor, with irinotecan (IRN) and temozolomide (TMZ) in neuroblastoma (NB). *J Clin Oncol.* 2010;**28**:10593.

29 DuBois SG, Marachelian A, Fox E, et al. Phase I Study of the Aurora A Kinase Inhibitor Alisertib in Combination With Irinotecan and Temozolomide for Patients With Relapsed or Refractory Neuroblastoma: A NANT (New Approaches to Neuroblastoma Therapy) Trial. *J Clin Oncol* 2016;**34**:1368–75.

30 Gustafson WC, Meyerowitz JG, Nekritz EA, et al. Drugging MYCN through an allosteric transition in Aurora kinase A. *Cancer Cell* 2014;**26**:414–27.

31 Du J, Yan L, Torres R, et al. Aurora A-Selective Inhibitor LY3295668 Leads to Dominant Mitotic Arrest, Apoptosis in Cancer Cells, and Shows Potent Preclinical Antitumor Efficacy. *Mol Cancer Ther* 2019;**18**:2207–19.

32 Filippakopoulos P, Qi J, Picaud S, et al. Selective inhibition of BET bromodomains. *Nature* 2010;**468**:1067–73.

33 Puissant A, Frumm SM, Alexe G, et al. Targeting MYCN in neuroblastoma by BET bromodomain inhibition. *Cancer Discov* 2013;**3**:308–23.

34 Wyce A, Ganji G, Smitheman KN, et al. BET inhibition silences expression of MYCN and BCL2 and induces cytotoxicity in neuroblastoma tumor models. *PloS one* 2013;**8**:e72967.

35 Bandopadhayay P, Bergthold G, Nguyen B, et al. BET bromodomain inhibition of MYC-amplified medulloblastoma. *Clin Cancer Res* 2014;**20**:912–25.

36 Ramadoss M, Mahadevan V. Targeting the cancer epigenome: synergistic therapy with bromodomain inhibitors. *Drug Discov Today* 2018;**23**:76–89.

37 Doroshow DB, Eder JP, LoRusso PM. BET inhibitors: a novel epigenetic approach. *Ann Oncol* 2017;**28**:1776–87.

38 Felgenhauer J, Tomino L, Selich-Anderson J, Bopp E, Shah N. Dual BRD4 and AURKA Inhibition Is Synergistic against MYCN-Amplified and Nonamplified Neuroblastoma. *Neoplasia* 2018;**20**:965–74.

39 Cancer M, Drews LF, Bengtsson J, et al. BET and Aurora Kinase A inhibitors synergize against MYCN-positive human glioblastoma cells. *Cell Death Dis* 2019;**10**:881.

40 Iniguez AB, Alexe G, Wang EJ, et al. Resistance to Epigenetic-Targeted Therapy Engenders Tumor Cell Vulnerabilities Associated with Enhancer Remodeling. *Cancer Cell* 2018;**34**:922–38 e7.

41 Yogev O, Barker K, Sikka A, et al. p53 Loss in MYC-Driven Neuroblastoma Leads to Metabolic Adaptations Supporting Radioresistance. *Cancer Res* 2016;**76**:3025–35.

42 Mathews Griner LA, Guha R, Shinn P, et al. High-throughput combinatorial screening identifies drugs that cooperate with ibrutinib to kill activated B-cell-like diffuse large B-cell lymphoma cells. *Proc Natl Acad Sci U S A* 2014;**111**:2349–54.

43 Chen L, Wilson K, Goldlust I, et al. mQC: A Heuristic Quality-Control Metric for High-Throughput Drug Combination Screening. *Sci Rep* 2016;**6**:37741.

44 Bliss CI. The Toxicity of Poisons Applied Jointly. *Annals of Applied biology* 1939;**26**:585–615.

45 Michaelis M, Selt F, Rothweiler F, et al. Aurora kinases as targets in drug-resistant neuroblastoma cells. *PloS one* 2014;**9**:e108758.

46 Bogen D, Wei JS, Azorsa DO, et al. Aurora B kinase is a potent and selective target in MYCN-driven neuroblastoma. *Oncotarget* 2015;**6**:35247–62.

47 Morozova O, Vojvodic M, Grinshtein N, et al. System-level analysis of neuroblastoma tumor-initiating cells implicates AURKB as a novel drug target for neuroblastoma. *Clin Cancer Res* 2010;**16**:4572–82.

48 Lin CY, Loven J, Rahl PB, et al. Transcriptional amplification in tumor cells with elevated c-Myc. *Cell* 2012;**151**:56–67.

49 Zeid R, Lawlor MA, Poon E, et al. Enhancer invasion shapes MYCN-dependent transcriptional amplification in neuroblastoma. *Nat Genet* 2018;**50**:515–23.

50 Carr-Wilkinson J, O'Toole K, Wood KM, et al. High Frequency of p53/MDM2/p14ARF Pathway Abnormalities in Relapsed Neuroblastoma. *Clin Cancer Res* 2010;**16**:1108–18.

51 Xue C, Haber M, Flemming C, et al. p53 determines multidrug sensitivity of childhood neuroblastoma. *Cancer Res* 2007;**67**:10351–60.

52 Keshelava N, Zuo JJ, Chen P, et al. Loss of p53 function confers high-level multidrug resistance in neuroblastoma cell lines. *Cancer Res* 2001;**61**:6185–93.

53 Mazar J, Gordon C, Naga V, Westmoreland TJ. The Killing of Human Neuroblastoma Cells by the Small Molecule JQ1 Occurs in a p53-Dependent Manner. *Anticancer Agents Med Chem* 2020.

54 Gerlach D, Tontsch-Grunt U, Baum A, et al. The novel BET bromodomain inhibitor BI 894999 represses super-enhancer-associated transcription and synergizes with CDK9 inhibition in AML. *Oncogene* 2018;**37**:2687–701.

55 Bolin S, Borgenvik A, Persson CU, et al. Combined BET bromodomain and CDK2 inhibition in MYC-driven medulloblastoma. *Oncogene* 2018.

56 Ackermann S, Cartolano M, Hero B, et al. A mechanistic classification of clinical phenotypes in neuroblastoma. *Science* 2018;**362**:1165–70.

57 Eleveld TF, Oldridge DA, Bernard V, et al. Relapsed neuroblastomas show frequent RAS-MAPK pathway mutations. *Nat Genet* 2015;**47**:864–71.

58 Maris JM, Morton CL, Gorlick R, et al. Initial testing of the aurora kinase A inhibitor MLN8237 by the Pediatric Preclinical Testing Program (PPTP). *Pediatr Blood Cancer* 2010;**55**:26–34.